Paw Inflammation and Bone Lesions Detection in Psoriatic Arthritis Using Non-invasive Fluorescence and X-ray Imaging

Robin-Jagerschmidt, C[1]; Cauvin, A.[1]; Chanudet, E.[1]; Marsais, F.[1]; Auberval, M.[1] and Yudina, A.[2]

[1] Galapagos SASU 102, avenue Gaston Roussel, 93230 Romainville, France

[2] Bruker BioSpin, 34 rue de l'Industrie, 67166 Wissembourg, France

Overview

Patients with Psoriatic Arthritis (PsA) often present a complex of clinical features, including: Arthritis in the peripheral joints, inflammation of the entheses, (at the junction of tendon to bone), bone erosion and new bone formation leading to dactylitis.

Serum concentration of IL-23 is reported to be elevated in patients with ankylosing spondylitis. Recently, overexpression of IL-23 in mice has been shown to lead to axial and peripheral enthesitis, as well as new bone formation by acting on resident T cells[1]. Here we apply and characterize a preclinical model of PsA induced by systemic IL-23 expression in mice. Follow up and quantification of inflammation and bone lesions were demonstrated by means of dual fluorescence and X-Ray imaging.

Materials & Methods

A quantity of 3 µg mcIL-23 enhanced Episomal Expression Vector (IL-23 EEV, SBI) was injected into 8 week-old B10. RIII male mice (Charles River, France) by hydrodynamic i.v. injection[2]. Control animals received Ringer solution.

Circulating levels of IL-23 were measured at 5 days post injection (Mouse IL-23 Quantikine ELISA Kit, R&D systems). Inflammation of the paw and fingers were scored according to Sherlock et al.[1]. Inflammation and new bone formation were assessed with *in vivo* non-invasive molecular imaging, using ProSense680™ and OsteoSense750EX™ probes (Perkin Elmer, France), respectively. Images were captured using the Bruker In-Vivo Xtreme imaging system (Bruker BioSpin, France). Bone damage and dactylitis were confirmed using high magnification X-ray imaging (Bruker In-Vivo Xtreme imaging system with magnification stage). At the terminal endpoint, hind limbs were collected for histology analysis.

In vivo Fluorescence and X-ray Imaging

At 24 hours before imaging, probes were administered to mice (0.8 nmol/10 g, i.p.) according to the workflow shown in Table 1

Day	Group 1 (control)	Group 2 (mIL23)
0	Ringer hydrodynamic delivery	IL 23 EEV hydrodynamic delivery
5	Blood sampling for IL 23 assay	
7	ProSense™ *in vivo* imaging	
21	ProSense™ *in vivo* imaging	
35	X-ray *in vivo* imaging with magnification stage	
43	ProSense™ / OsteoSense™ / X-ray *in vivo* imaging	

Table 1: Experimental workflow

In preparation for imaging, mice were anesthetized with Imalgene and Rompun (7.5 % / 2.5 %; 0.1 mL/10 g, i.p.).

Granulocyte infiltration and bone remodeling were measured using a Bruker In-Vivo Xtreme imaging system, equipped with a deeply cooled 4 MP CCD camera. Fluorescent images were acquired with the following camera settings: 5 sec acquisition time, f-stop 1.1, and 2x2 binning. For imaging ProSense680™ a 630 nm (+/- 10 nm) excitation and, 700 nm (+/- 17.5 nm) wide-angle emission filter set was chosen. For imaging OsteoSense750EX™ a 720 nm (+/- 10 nm) excitation, and 790 nm (+/- 20 nm) emission filter selection was applied.

For anatomical co-registration, an X-ray image at 1.2 sec acquisition time, f-stop 2.8, binning 1 x 1, X-ray filter 0.2 mm and with an X-ray energy of 45 kVp was performed. All images were taken with a 190 mm x 190 mm field of view (FOV).

For the analysis of bone damage and dactylitis, mice were assessed using X-ray imaging with magnification stage of the Bruker In-Vivo Xtreme at 10 sec acquisition time, f-stop 2, 1 x 1 binning, 0.4 mm X-ray filter, X-ray energy 45 kVp.

Image Analysis and Presentation

Signal intensity analysis was performed using Molecular Imaging Software version 7.1 (Bruker BioSpin, Billerica, MA, USA). A free form Region of interest (ROI) was drawn around forelimbs and hind limbs. Based on the control mouse images of Group 1, a fluorescence signal dynamic range threshold of 400 AU was selected. ROI data were exported and saved to Microsoft Excel® files, while images were exported as JPEG files.

Histology:

At sacrifice, the hind paws were fixed in buffered 10% formalin, decalcified, paraffin embedded and sectioned. For each paw, one 4 µm thick section every 10 sections was collected and stained with hematoxylin-eosin (HE) and one adjacent section was stained by IHC using anti-MPO for neutrophil detection.

Statistical Analysis

For each ROI, the signal mean and standard error to the mean (s.e.m.) were calculated. A statistically significant difference between the study groups was evaluated with Prism® software using a one-way ANOVA followed by a Dunnett's multiple comparisons post-hoc test. In Figures presented here, the statistical significance level observed was symbolized as follows: * = p<0.05; ** = p<0.01; *** = p<0.001.

Results/Discussion

From day 8 onwards an IL23-induced swelling of paw and fingers could be observed and which is in line with findings

Figure 1

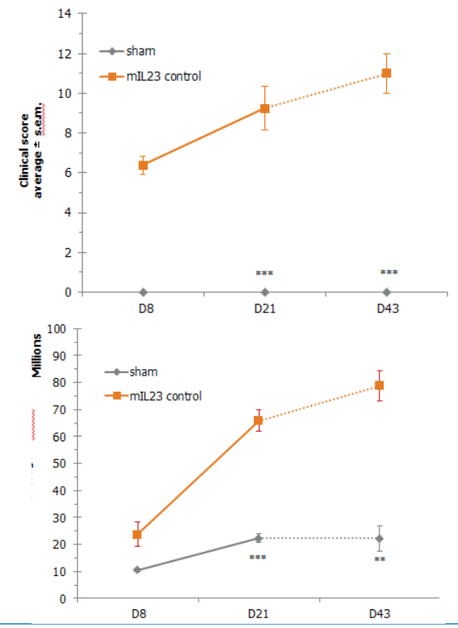

Figure 1: Clinical scoring and inflammation measured by *in vivo* molecular imaging. Upper panel: inflammation of the paw and fingers were scored according to Sherlock et al.[1]. Lower panel: images were taken at days 8, 21 and 43, respectively, following injection of Ringer (sham group) or IL-23 EEV (mIL23 control). Mice were imaged for 5 sec, 24 hours following administration of ProSense680™ probe (0.8 nmol /10 g, i.p.). ** = p<0.01; *** = p<0.001.

from Sherlock et al.[1] (Figure 1, upper panel). Follow-up of the inflammatory process was assessed also using non-invasive molecular *in vivo* imaging (Figure 1 lower panel). Good correlation was observed between PsA clinical scores of mice and granulocyte infiltration (Figure 1). In addition, localization of the fluorescence around the heel was compatible with inflammatory pathology focused on the entheses as reported previously1 and thus represent the molecular footprint of IL23-induced swelling (Figure 2).

Figure 2

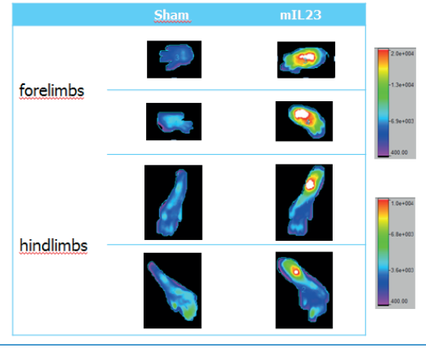

Figure 2: Illustration of inflammation of forelimbs and hind limbs measured by *in vivo* molecular imaging with the ProSense680™ probe.

In the later phase of the disease, bone lesion and dactylitis, both hallmarks of the disease, were clearly visible before sacrifice. Planar 2D X-ray imaging has demonstrated micro-calcifications at these sites displaying highest bone formation and remodeling (Figure 3).

Figure 3

Figure 3: Visualization of osteophyte-derived bone remodeling at day 35 using X-ray *in vivo* imaging with magnification stage on the In-Vivo Xtreme.

In addition to classically 2D planar X-ray image analysis of bone remodeling the use of molecular fluorescence markers clearly visualized the molecular process via non-invasive *in vivo* imaging (Figure 4). While the sham animal represented the baseline, the IL23-induced swelling was clearly observable several magnitudes difference in signal intensity.

Figure 4

Figure 4: Illustration of bone remodeling of hind limbs measured by *in vivo* molecular imaging with the OsteoSense750™ probe.

Post sacrifice, histological analysis identified psoriatic arthritis hallmarks. Inflammatory features were focused on the enthesis and the periosteum, with severe entheseal inflammation (Figure 5) expansion of periosteal osteoblasts (Figure 6).

Figure 5

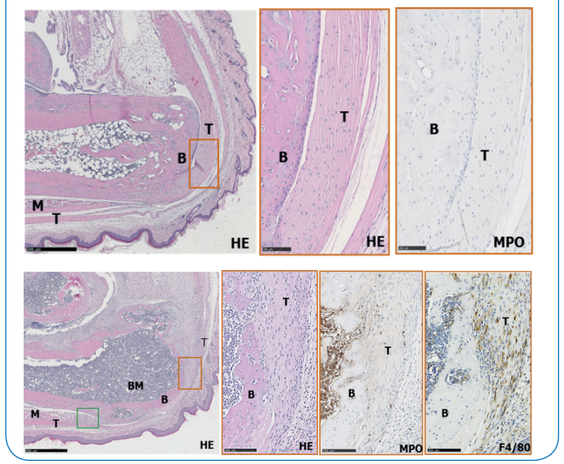

Figure 5: Microscopic images of Achilles' tendon and enthesis
Representative sections post HE staining from heels of sham (upper panel) and mc IL-23 (lower panel) mice. Anti-MPO IHC gave a brown staining of neutrophil and macrophage, respectively.
M: muscle, T: tendon, B: bone, BM: bone marrow.

Figure 6

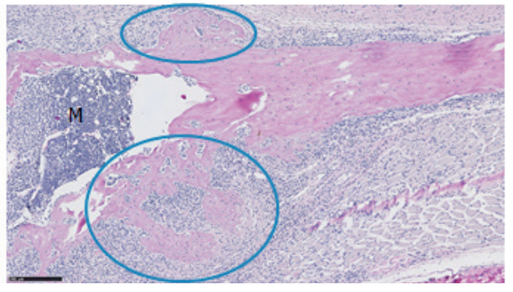

Figure 6: Microscopic images of new bone formation
Representative sections post-HE staining from heels of mc IL-23 mice. Anti-MPO IHC gave a brown staining of neutrophils and macrophages, respectively.
M: metatarsal new bone formation areas are circled in blue

Conclusion

In vivo fluorescence imaging in combination with high resolution, low dose X-ray together provided a sensitive, non-invasive approach for the detection of inflammation and bone damage processes in a preclinical model of PsA, induced by systemic IL-23 expression in mice. These data were supported by a clinical gold-standard as well as histopathology analysis. The non-invasive model characterisation of PsA processes introduced here, provides future investigations a new, high throughput experimental platform for conducting rapid, statistically robust evaluations of therapy/new therapy combinations in the field of PsA.

References

[1] Sherlock JP, Joyce-Shaikh B, Turner SP, Chao CC, Sathe M, Grein J, Gorman DM, Bowman EP, McClanahan TK, Yearley JH, Eberl G, Buckley CD, Kastelein RA, Pierce RH, Laface DM, Cua DJ. IL-23 induces spondyloarthropathy by acting on ROR-γt+ CD3+CD4-CD8- entheseal resident T cells (2012) Nature Med 7:1069–1076

[2] Liu F, Song YK and Liu D. Hydrodynamics-based transfection in animals by systemic administration of plasmid DNA (1999) Gene Therapy 6:1258–1266

Bruker BioSpin

info@bruker.com
www.bruker.com